Practical Issues in the Use of NdFeB Permanent Magnets in Maglev, Motors, Bearings and Eddy Current Brakes

Marc T. Thompson, Member, IEEE

Thompson Consulting Inc., 9 Jacob Gates Road, Harvard, MA 01451, phone: (978) 456-7722, fax: (240) 414-2655, email: marctt@thompsonrd.com , web: www.thompsonrd.com

Electrical and Computer Engineering Department, Worcester Polytechnic Institute, 100 Institute Road, Worcester, MA 01609, email: marctt@wpi.edu

Abstract---In this paper, practical design issues related to the use of high-strength neodymium-iron-boron (NdFeB) magnets are described. These magnets have increasing utility in transportation systems (Maglev, linear and rotary motors), bearings, and in eddy-current brakes.   However, careful design must be done to utilize the full capabilities of these magnets.

Keywords---Neodymium-iron-boron, NdFeB, permanent magnets, motors, eddy current brakes, linear motors, magnetic circuits, Halbach array, permeance, bearings, EMS, EDS, linear synchronous motor, electromagnetic levitation, electrodynamic levitation.

NOMENCLATURE

Item	Description	Units
α	Temperature coefficient of B_r	$^oC^{-1}$
β	Temperature coefficient of H_{ci}	$^oC^{-1}$
σ_{NdFeB}	Electrical conductivity of NdFeB	$\Omega^{-1}m^{-1}$
Φ_m	Magnetic flux inside a permanent magnet	Weber
$\mathfrak{R}$	Magnetic reluctance	A-turns/Weber
μ_o	Magnetic permeability of free space	$4\pi\times10^{-7}$ H/m
μ_m	Recoil permeability of a permanent magnet	H/m
μ_r	Relative recoil permeability	---
λ	Magnetic wavelength	m
A_g	Cross-sectional area of airgap	m^2
A_m	Cross-sectional area of permanent magnet	m^2
B_g	Airgap magnetic flux density	T
B_m	Operating point of permanent magnet flux density	T
B_r	Remnant magnetic flux density	T
B_{ro}	Remnant magnetic flux density at temperature T	T
D	Magnet height	m
f_b	Braking force generated by an eddy current brake	N
$F_{b,max}$	Maximum braking force generated by an eddy current brake at v_{pk}	N
g	Airgap length	g
H_c	Coercive force	A/m
H_{ci}	Intrinsic coercive force	A/m
H_{cio}	Intrinsic coercive force at temperature T	A/m
H_m	Magnetic field inside a permanent magnet	A/m
l_m	Length of permanent magnet	m
l_p	Magnetic path length in steel	m
N	Number of blocks per wavelength in Halbach array	---
N_{lam}	Number of laminations	---
v	Linear velocity	m/s
v_{pk}	Velocity at which force peaks in an eddy current brake	m/s

I. INTRODUCTION

This year (2008 at the time of this writing) marks the 25th anniversary of the introduction of sintered neodymium-iron-boron (NdFeB) magnets. In 1983, this new generation of rare-earth magnet was introduced and patented independently by Sumitomo Special Metals and General Motors (later Magnequench). Sumitomo and Magnequench later cross-licensed their patents. In subsequent years, the NdFeB divisions of GE and Sumitomo were bought and sold several times; the current incarnations are Neomax (a 2003 merger of Hitachi and Sumitomo Specialty Metals) and the Magnequench division of AMR Technologies which became Neo Material Technologies in 2005.

In the past 20 years or so, significant improvements have been made in the magnetic strength and thermal stability of these permanent magnet materials [1]-[6] opening up new applications in large-scale systems such as motors, bearings, Maglev and eddy current brakes as well as other transportation applications such as hybrid vehicles. A key figure of merit is the maximum energy product, given in megaGauss-Oersteds (MGOe), but equally important are the issue of thermal stability and the resistance of the permanent magnets to demagnetization. Currently, NdFeB with maximum energy product of greater than 50 MGOe is commercially available [7]. NdFeB is replacing samarium cobalt (SmCo) and alnico in many applications, but for very high-temperature applications, SmCo is still a competitor to NdFeB. This paper focuses on the use of high-strength NdFeB magnets in large-scale applications where temperatures are modest, and describes some of the design challenges unique to NdFeB design, including specifically mechanical and thermal design issues.

II. ANALYTICAL APPROXIMATE MODELING OF NDFEB SYSTEMS

A. Use of Ampere's and Gauss' laws and load line

NdFeB magnets have the characteristic B/H curve shown in Fig. 1a where B_m is the flux density inside the magnet and H_m is the magnetic field inside the magnet. Material parameters (which are further discussed in following sections) are the coercive force (H_c, with units of A/m) and remnant flux density (B_r, with units of Tesla). The permanent magnet constrains the operating point (B_m, H_m) of the magnet to be somewhere on the line shown. By constructing a load line by analyzing the external circuit surrounding the magnet, we can predict the operating point of the magnet at the intersection of the magnet B/H curve with the load line.

We'll consider the magnetic circuit of Fig. 1b. The permanent magnet has length l_m and cross-sectional area A_m and is wrapped with high-permeability steel. The steel has magnetic path length l_p, and an airgap of length g is also shown. Using Ampere's law around the dashed path (and noting that our approximation of infinite permeability

assures that magnetic field H = 0 in the steel) we note:

$$H_m l_m + H_g g = 0 \quad \text{[Eq. 1]}$$

where H_g is the magnetic field in the airgap. Next we use Gauss' magnetic law which says that flux is continuous around a loop, to get:

$$B_m A_m = B_g A_g \quad \text{[Eq. 2]}$$

where A_g is the cross-sectional area of the airgap. Noting that the airgap flux density $B_g = \mu_o H_g$, we next solve for B_m as a function of H_m, resulting in the load line equation:

$$B_m = -\mu_o \left(\frac{l_m A_g}{g A_m} \right) H_m \quad \text{[Eq. 3]}$$

We plot the load line on the magnet B/H curve resulting in Fig. 1c. We see the intuitive result that the operating point of the magnet is at a higher B_m if the magnet is longer or if the airgap is smaller. Conversely, if the airgap grows, the magnetic flux density produced by the magnet is lower and the airgap flux density is lower.
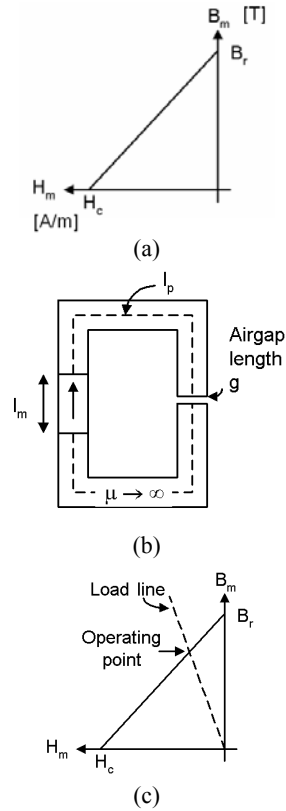

(a)

(b)

(c)

Fig. 1. Construction of a load line in a circuit containing a NdFeB magnet and steel. (a) Characteristic demagnetization B/H curve of the magnet. (b) A magnetic circuit containing a permanent magnet, high-permeability steel and an airgap. (c) Load line showing operating point of the permanent magnet

The magnetic flux density predicted by the load line method, and following methods, is approximate and should be used with care.

B. Magnetic circuits

Rough order-of-magnitude modeling of the amplitude of the magnetic field produced by a high-strength magnet can be done by using magnetic circuit modeling in cases where airgaps are relatively small. Using magnetic circuit modeling, magnetomotive force (MMF) is analogous to voltage, flux (Φ) is analogous to current, and the proportionality constant relating MMF and flux is magnetic "reluctance." The magnetic circuit model of a permanent magnet (Fig. 2a) of length l_m and cross sectional area A_m is shown in Fig. 2b. The MMF source is $H_c l_m$ where H_c is the coercive force of the magnet. The magnetic reluctance inside the magnet is given by:

$$\Re_m = \frac{l_m}{\mu_m A_m} \quad \text{[Eq. 4]}$$

where $\mu_m \approx \mu_o$ is the recoil magnetic permeability of the permanent magnet material.

A closed magnetic circuit is shown in Fig. 2c, where we see a permanent magnet, steel (with 6 labeled legs), and an airgap. Using magnetic circuit analysis, we replace each leg and airgap with reluctances of value:

$$\Re = \frac{Path\ length}{\left(\mu\right)\left(Cross\ sectional\ area\right)} \quad \text{[Eq. 5]}$$

Next, we approximate the magnet flux density (Φ_m) and airgap flux B_g as:

$$\Phi_m \approx \frac{H_c l_m}{\Re_m + \Re_1 + \Re_2 + \Re_3 + \Re_g + \Re_4 + \Re_5 + \Re_6} \quad \text{[Eq. 6]}$$

$$B_g \approx \frac{\Phi_m}{A_g}$$

where A_g is the cross sectional area of the airgap. Note that this is an approximate method, which ignores leakage flux and 3D end effects, but is useful for generating rough estimates of flux density. The reluctances of leakage paths can be approximated by adding other reluctances to the circuit model [8]-[9] to model flux leakage through the air.
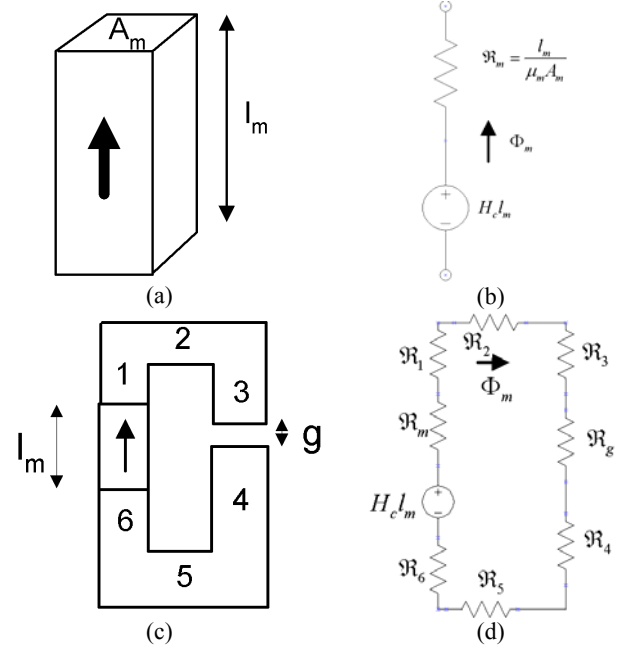

Fig. 2. Magnetic circuit modeling of a permanent magnet. (a) Geometry of a permanent magnet. (b) Magnetic circuit model of a PM. (c) Closed magnetic circuit with steel and an airgap. (d) The magnetic circuit model

C. Method of images

We can use the method of images to simplify the analysis of structures containing permanent magnets where there are magnet-steel interfaces. Referring to the structure of Fig. 3a, we see a permanent magnet of length l_m attached to a piece of steel with high magnetic permeability. The boundary condition at the plane defining the magnet-steel interface is that the magnetic field is perpendicular to the steel, assuming that the magnetic permeability of the steel is much higher than that of free space, and that the steel doesn't saturate. Above the steel, the field lines can be calculated using an equivalent circuit, with permanent magnet of length $2l_m$ (Fig. 3b).

Fig. 3. Method of images. (a) Permanent magnet on top of a piece of steel. (b) Equivalent circuit using method of images for prediction of magnetic field above the steel surface.

D. Halbach array

The 2D linear Halbach array (Fig. 4a) is a magnetic structure where the magnetization vector rotates, producing one side of the array with a strong field, and a second side that has a weak magnetic field. This array was

first described by J. C. Mallinson in 1973 [10] as a one-sided flux "magnetic curiosity" and soon after discovered independently by Klaus Halbach [11]-[12] for use in particle accelerators at Lawrence Livermore National Laboratory. Halbach arrays have been proposed for use in linear motors [13]-[14], rotary motors [15], Maglev levitation [16]-[17], eddy current brakes [18], and high field magnets [19] and variations are also used in other products such as flexible refrigerator magnets

   An ideal Halbach array has a magnetic vector which rotates continuously along the length of the array. This ideal array has a magnetic flux density on the strong side which varies sinusoidally with distance, and zero field on the weak side. However, Halbach arrays are generally built with discrete magnets with the ideal magnetization pattern being approximated in a piecewise fashion. For an intuitive explanation of how the Halbach array produces these strong-side and weak-side fields by constructive and destructive interference of the fields from the individual blocks, see [20]

   A design parameter of the Halbach array is the number N, which is the number of blocks per wavelength in the array. Another design parameter is the block thickness D. In Fig. 4a, we see an N = 8 Halbach array where the magnet vector rotates 45° per block. The blocks in the array need not be necessarily square; in Fig. 4b we see an FEA model [21] of an N = 8 Halbach array made with magnets with rectangular cross section. These structures lend themselves to closed-form 2D solutions, but 3D end effects do significantly alter the amplitude of the fields near the ends of the array and outside the airgaps. Also, near the ends of the array the weak-side field is higher than the 2D analysis predicts, also due to 3D effects [22].
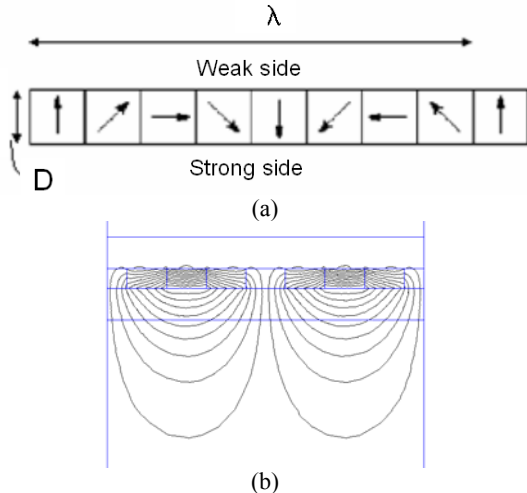

(a)

(b)

Fig. 4. Linear Halbach array. (a) Magnet structure of N = 8 Halbach array with wavelength λ and block thickness D. (b) 2D FEA model showing flux lines of N = 8 Halbach array with wavelength λ = 200 mm, block width = 25 mm and block thickness D = 12.5 mm.

   The strong side (1st harmonic) peak magnetic flux density B of a single-sided Cartesian Halbach array is

given by:

$$B = B_r F_1 F_2 e^{-\frac{2\pi y}{\lambda}}$$

$$F_1 = \frac{\sin\left(\frac{\pi}{N}\right)}{\left(\frac{\pi}{N}\right)} \quad \text{[Eq. 7]}$$

$$F_2 = 1 - e^{-\frac{2\pi D}{\lambda}}$$

where y is the distance from the strong side surface, λ is the magnetic wavelength, and D is the block thickness. The first harmonic of the weak-side field is eliminated, and the dominant weak-side harmonic is the 3rd for the N = 4 array (Fig. 5). For the N = 8 array, the dominant harmonic on the weak side is the 7th. Note that the weak side fields decay rapidly away from the magnet surface. Similar expressions can be derived for the cylindrical 2D Halbach array.
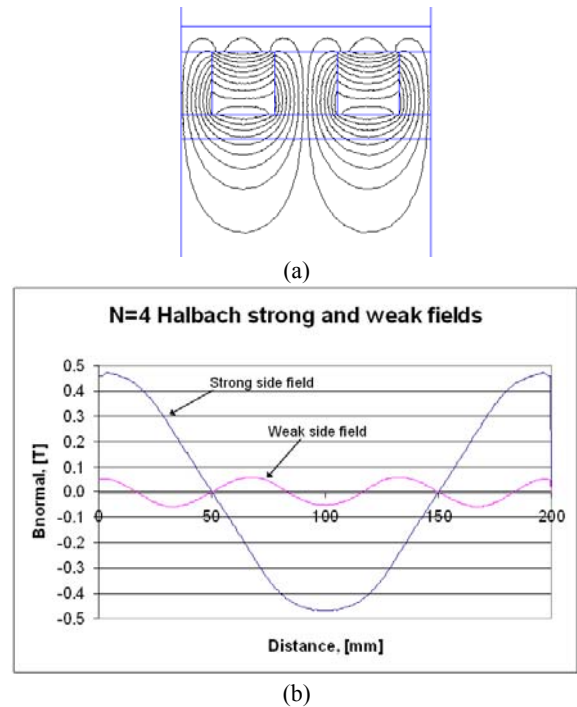

(a)

(b)

Fig.5. Linear Halbach array. (a) One wavelength of an N = 4 Halbach array, with square grade 40 permanent magnet blocks with λ = 200 mm and D = 50 mm. (b) Fields at a distance 20 mm from the strong side and weak sides. Note that the strong-side field has low harmonic content and that the weak-side field is dominated by the 3rd harmonic.

III. PRACTICAL DESIGN ISSUES WITH NDFEB PERMANENT MAGNETS

A. Demagnetization B/H curve of NdFeB at room temperature

   The B/H curve of one particular grade 40 NdFeB at room

temperature (Table 1) is shown in Fig. 6, where we see the parameters derived from manufacturer's data [23].

Table 1. Parameters for grade 40 NdFeB

B_r Remnant flux density = 1.27 T
H_c Coercive force = 905 kA/m
μ_r Relative permeability = 1.11

Note that the relative permeability $\mu_r = 1.11$ is the permeability in the direction of magnetization; the relative permeability is a little lower ($\mu_r \sim 1$) in directions orthogonal to the magnetization direction.
 NdFeB magnets exhibit a nearly linear B/H demagnetization curve in the second quadrant when operated at a modest temperature. When a permanent magnet is used in a magnetic circuit, it provides magnetic flux in an airgap which can provide forces. The operating point of the magnet occurs at the intersection of the demagnetization curve with the load line and the slope of the load line depends on details of the magnetic circuit surrounding the magnet as shown before. Operation of the magnet at the "maximum energy product" $(BH)_{max}$ point results in maximum ratio of airgap flux to magnet volume [24]. In many applications it is desirable to operate at $(BH)_{max}$ but in some applications it's necessary to operate off this optimum point.
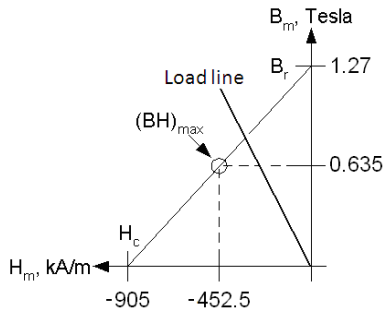

Fig. 6. B/H curve of grade N40 NdFeB, information from Arnold Magnetic Technologies [23]. Superimposed on the magnet B_m-H_m curve is a typical load line which depends on the detail of the external circuit surrounding the permanent magnet. The operating point of the magnet is the intersection of the magnet demagnetization curve with the load line, shown here at $B_m = 0.8T$ and $H_m = -334$ kA/m.

B. Effects of elevated temperature
   In high-temperature applications where maximum magnetic strength is required, SmCo is the magnet of choice. In lower temperature applications where high magnetic strength is necessary, NdFeB is a common choice. However, special care must be taken to ensure that irreversible demagnetization of the permanent magnet does not occur during assembly or during temperature cycling.
   The "Curie temperature" is the temperature at which the magnetization is totally destroyed. A typical Curie temperature for NdFeB is 300 ^{o}C, but for practical design

the magnet must be operated at temperatures significantly lower than this. This limitation is due to temperature coefficients of remnant flux density and intrinsic coercive force and the possibility of irreversible demagnetization if the temperature is too high or if the demagnetizing field is too high.
   The remnant flux density B_r and intrinsic coercive force H_{ci} of the magnets decrease with temperature. For higher energy product NdFeB magnets, the temperature effects are more pronounced [25]-[27]. The remnant magnetic flux density of the magnet decreases with increasing temperature as:

$$B_r(T) = B_{ro}\left[1 + \alpha(T - T_o)\right] \quad \text{[Eq. 8]}$$

where B_{ro} is the remnant magnetic flux density at temperature T_o and α is the temperature coefficient of the remnant flux density and is approximately -0.0012/^{o}C for grade 40 NdFeB [23]. The intrinsic coercive force of the magnet also decreases with increasing temperature, as:

$$H_{ci}(T) = H_{cio}\left[1 + \beta(T - T_o)\right] \quad \text{[Eq. 9]}$$

where H_{cio} is the intrinsic magnetic coercivity at temperature T_o and β is the temperature coefficient of the remnant flux density and is on order of -0.0065/^{o}C. If the temperature increase is modest, the demagnetization is reversed once the temperature reduces. However, if the operating temperature of the magnet increases above a critical temperature, the demagnetization is irreversible and some loss of magnetic strength results. The critical temperature depends on the temperature coefficients of the magnet and details of the magnetic load line as shown next.
   NdFeB magnet grades are denoted with a de-facto standard use of suffixes: the suffixes refer to the maximum operating temperature as recommended by the manufacturer (Table 2). These specifications must be used with extreme care; a recommended operating temperature does not guarantee that the material magnetization will survive at that temperature. Whether or not the magnet demagnetizes depends on the details of the surrounding magnetic circuit and the load line under which the magnet operates.

Table 2. NdFeB magnet grade suffixes

Suffix	Maximum recommended operating temperature
None	80 ^{o}C
M	100 ^{o}C
H	120 ^{o}C
SH	150 ^{o}C
UH	180 ^{o}C
EH	200 ^{o}C

   The demagnetization curves of two different types of grade 40 NdFeB materials with typical numbers for

temperature coefficients α and β are shown in Fig. 7. Referring to Fig. 7a, we see NdFeB material with a recommended maximum operating temperature of 80 ^oC. In order to avoid reversible demagnetization at temperatures higher than 60 ^oC or so, one must avoid operating the magnet past the "knee" with demagnetizing field $H_m < H_{ci}$. This knee is much more pronounced at higher temperatures. Operation of the magnet at an operating point beyond the knee of the demagnetization curve results in irreversible reversal of the magnetization within the material and resultant degradation in the performance in the machine in which the magnet is used.

The demagnetization curves at different temperatures for a more temperature-stable grade 40 NdFeB UH are shown in Fig. 7b, with a maximum recommended operating temperature of 180 ^oC. Operation of this magnet in the temperature less than ~150 ^oC results in reversible decrease in B_r and H_c, but no irreversible demagnetization.

A comparison of specifications of these two different sub-types of 40 MGOe is shown in Table 3. This shows that the system designer must be aware of temperature effects in different sub-grades of NdFeB magnets.

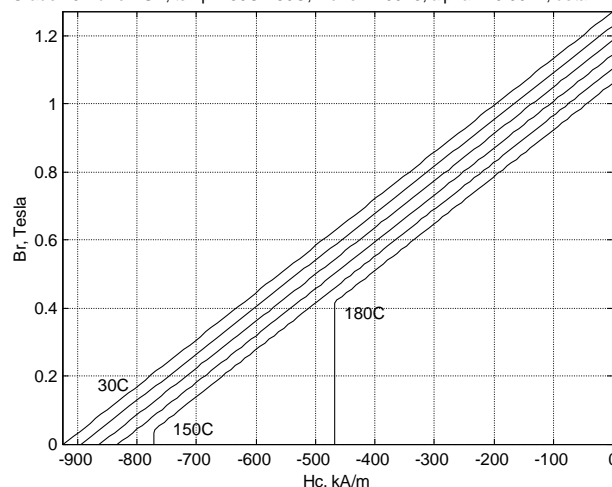**Table 3.** Comparison of specifications of grade N40 NdFeB with grade N40 UH

Item	Grade 40	Grade N40 UH
B_r	1.27 T	1.27 T
H_c	905 kA/m	925 kA/m
H_{ci}	955 kA/m	1990 kA/m
α	-0.0012	-0.0011
β	-0.0065	-0.0051
Max. working temp. as reported by manufacturer	80 ^oC	180 ^oC

Grade 40 NdFeB UH, temp = 30C-180C, mu-rel=1.0926, alpha = -0.0011, beta = -0.0051

(b)

Grade 40 NdFeB, temp = 30C-180C, mu-rel=1.1167, alpha = -0.0012, beta = -0.0065

(a)

Fig. 7. B/H curves of two subgrades of 40 MGOe NdFeB at room temperature, and up to 150C. (a) Assumed parameters for grade N40 are: B_r = 1.27T, H_c = 905 kA/m, H_{ci} = 955 kA/m, α = -0.0012 and β = -0.0065. Note the pronounced "knee" in the B/H curve at temperatures above ~90 ^oC. (b) Assumed parameters for grade N40 UH are: B_r = 1.27T, H_c = 925 kA/m, H_{ci} = 1990 kA/m, α = -0.0011 and β = -0.0051

C. Corrosion resistance

If NdFeB magnets are uncoated, oxidation at the surface results in surface oxidation, discoloration and degradation of the magnetic properties. NdFeB magnets need to be coated to prevent this corrosion. If magnets are uncoated, over time this oxidation results in loss of magnetic strength [28]. Fortunately, methods of coating are well-understood by magnet manufacturers who typically use anti-corrosion coatings such as nickel or epoxy resin.

D. Mechanical strength and magnet protection

It is recommended that NdFeB not be used as a main structural member in large machines, as the ultimate tensile strength (~12,000 psi) is significantly less than that of structural steel [29]. Furthermore, chipping, cracking and fracture can occur during grinding, assembly and even during operation of NdFeB magnets. For mechanical strength and protection it is common to use steel pole faces, steel backiron, nonmagnetic covers and/or epoxy potting of NdFeB magnet assemblies.

E. Assembly forces

When assembling NdFeB magnets, the assembly forces for large magnets are quite high and may require special tooling [30], [31]. Shown in Fig. 8 is a 2D finite-element model of two 2" cubic magnets, a typical size used in eddy current brakes and large linear motors and Maglev systems. The forces with the magnets in attraction and repulsion vs. airgap are shown in Fig. 8 where we see that the force at small airgaps approaches 200 pounds force, with the forces for magnets in repulsion and attraction

being comparable in magnitude. Note that 3D end effects are quite pronounced and the actual forces may be significantly lower.
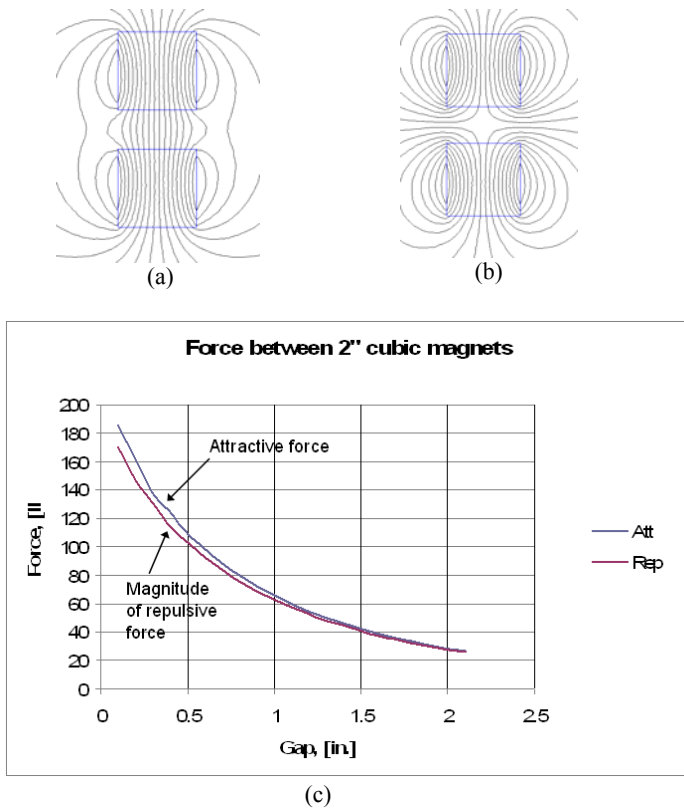

(a)   (b)

(c)

Fig. 8. 2D FEA model prediction of force between grade 40 NdFeB magnet cubes (a) Flux line plot of 2" magnets in attraction with 1" airgap between them (b) 2" magnets in repulsion (c) Magnitude of force (in lbf, pounds-force) vs. airgap as the airgap is varied from 0.1" to 2.1" showing force greater than 100 lbf at small airgap.

F. Stray magnetic fields

There are significant stray magnetic fields that extend far away from the surface of high strength NdFeB magnets. For fields greater than 50 Gauss or so, damage can occur to credit cards and steel tools or other permanent magnets can be pulled toward the magnet.

Shown in Fig. 9, we see the flux line plot for a cylindrical grade 40 NdFeB magnet with vertical magnetization. The semicircles are at distances of 6", 12" and 24" from the center the magnet cylinder. At a distance r = 6", the maximum flux density is 0.05 Tesla (500 Gauss). At r = 12" the maximum field is 60 Gauss and at r = 24" the maximum flux density has dropped to 7.5 Gauss. We note that far away from the magnet, the magnetic field is approximated as a dipole with a field rolloff with radial distance of $1/r^3$.

One stringent limit for stray magnetic fields are the ICNIRP guidelines [32], which give a recommended maximum field of 5 Gauss for DC fields for pacemaker wearers, and 40 Gauss for the general public. During shipping, it is typical for high strength magnets to be

packaged in shielded shipping boxes, with shielding being provided by thin sheets of steel surrounding the permanent magnets. The permanent magnets are separated by non-magnetic "keepers."
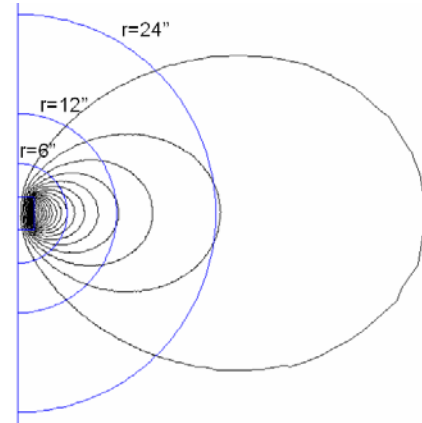

Fig. 9. Flux lines from a grade 40 NdFeB cylindrical permanent magnet by axisymmetric 2D FEA. Magnet height h = 2" and magnet diameter = 2". One-half of the solution is shown. The semicircles are at r = 6", 12" and 24"

G. Finite electrical conductivity

NdFeB magnets have electrical conductivity of $\sigma_{NdFeB} \approx 0.7 \times 10^6$ $\Omega^{-1}m^{-1}$ (about 1% of copper [23]), and this conductivity is non-negligible. In applications where the permanent magnet is subjected to a time-varying magnetic field (e.g. in a motor or a generator) it may be necessary to laminate the magnet to avoid losses, self-heating and possible demagnetization due to induced eddy currents [33]. It can be shown [34, pp. 402] that laminating a permanent magnet operating in a uniform, time-varying field with N_{lam} slices reduces the total power dissipation in the magnet due to eddy currents by a factor of $\sim 1/(N_{lam})^2$.

IV. SOME SYSTEMS USING NDFEB MAGNETS

A. *Maglev and linear motors*

Today's NdFeB magnets are magnetically strong enough, and thermally stable enough to be used in linear motors and levitation systems for Maglev. Two Maglev systems using NdFeB magnets are under development in the U.S. under the Federal Transit Administration (F.T.A.) "Urban Maglev" program. The systems are the Magnemotion [35] M3 system (Acton MA), and the General Atomics [36]-[38] system (San Diego, CA). The systems each use significant quantities of NdFeB magnets in their levitation and propulsion systems.

The Magnemotion system uses NdFeB permanent magnets for electromagnetic levitation, with control electromagnets operating to stabilize the "EMS" magnetic suspension (Fig. 10). In an EMS suspension, magnets are attracted to steel, producing levitation. A long-stator linear

synchronous motor provides propulsion, working against NdFeB magnets on the moving chassis. The permanent magnets provide the bulk of the lift force, resulting in a suspension with minimal power consumption.
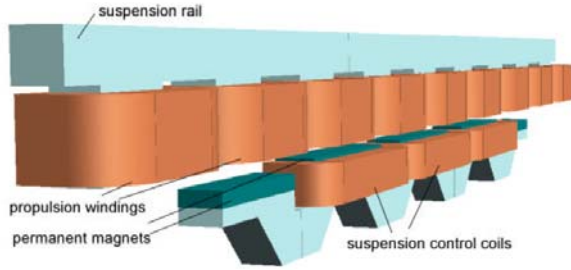

Fig. 10. The Magnemotion propulsion, levitation and guidance system as reported in the F.T.A. report on Urban Maglev.

   The General Atomics system uses two Halbach arrays of NdFeB magnets to levitate over a Litz-wire ladder track, in an electrodynamic, or "EDS" maglev system (Fig. 11). In EDS suspensions, repulsive or shear forces levitate the vehicle. A long-stator linear synchronous motor provides propulsion, working against a third Halbach array. Features of the EDS system are the finite magnetic drag force which needs to be overcome by the propulsion system, and the fact that no active control system is needed to stabilize the vertical suspension. However, the primary magnetic suspension is underdamped and damping must be implemented in a practical EDS system.
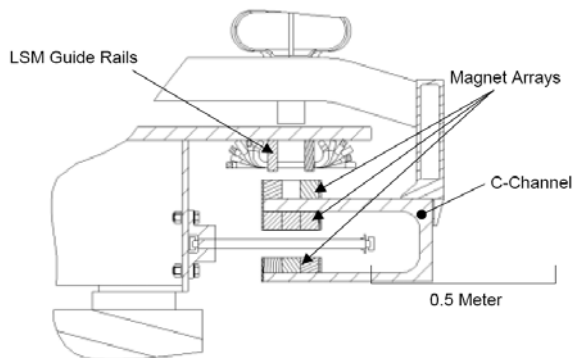

Fig. 11. View of the General Atomics propulsion, and levitation system as reported in the F.T.A. report on Urban Maglev.

B. Bearings

   NdFeB magnets are used in axial and radial bearings. One such bearing is shown in Fig. 12, a prototype built for NASA [39] in a flywheel energy storage project for satellites. Permanent magnets provide levitation and guidance forces. By Earnshaw's theorem [40] this suspension is unstable in at least one degree-of-freedom unless there is some mechanical constraint or active

closed-loop control, so there is a gap sensor and control electromagnet coils. A synchronous motor-generator speeds up the flywheel during motor mode, and generates electricity during times when power is needed.
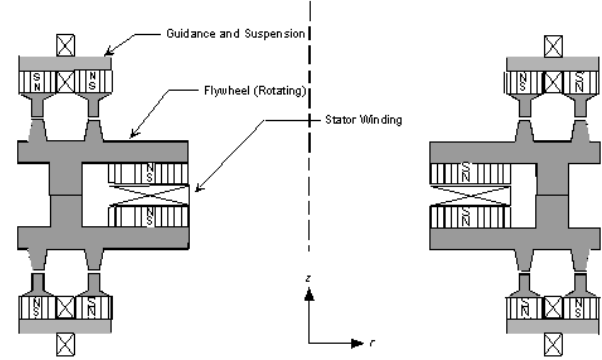

Fig. 12. Magnetically-levitated flywheel motor/generator for NASA project on satellite energy storage.

C. Permanent magnet eddy current brakes

   Eddy current brakes using permanent magnets are in use in amusement devices worldwide. Shown in Fig. 13a is the magnet assembly of a permanent magnet eddy current brake [41], [42]. Permanent magnets create a high field (~1T) in an airgap shown in Figure 13b in a brake installed in Hollywood, CA. A moving conducting fin traveling through the airgap has a high magnetic field impinging on it. By Faraday's law, there is an induced eddy current in the conducting fin, and these eddy currents generate a velocity-dependent braking force f_b, given by [43]:

$$f_b = 2F_{b,\max}\left(\frac{vv_{pk}}{v^2 + v_{pk}^2}\right) \quad \text{[Eq. 10]}$$

where v is relative velocity between the conductor and the permanent magnets, $F_{b,\max}$ is the maximum braking force, and v_{pk} is a characteristic velocity at which the braking force peaks. Shown in Fig. 13c is a 3D FEA model showing the braking force as a function of velocity for an eddy current brake with a 3/8" thick conducting fin. The braking force shows a characteristic peak at velocity v_{pk}. At low speed ($v \ll v_{pk}$), the braking force increases nearly linearly with velocity. This curve is entirely analogous with the induction machine [34] force-speed curve, whose operation is based on similar electrodynamic principles of induced eddy currents.
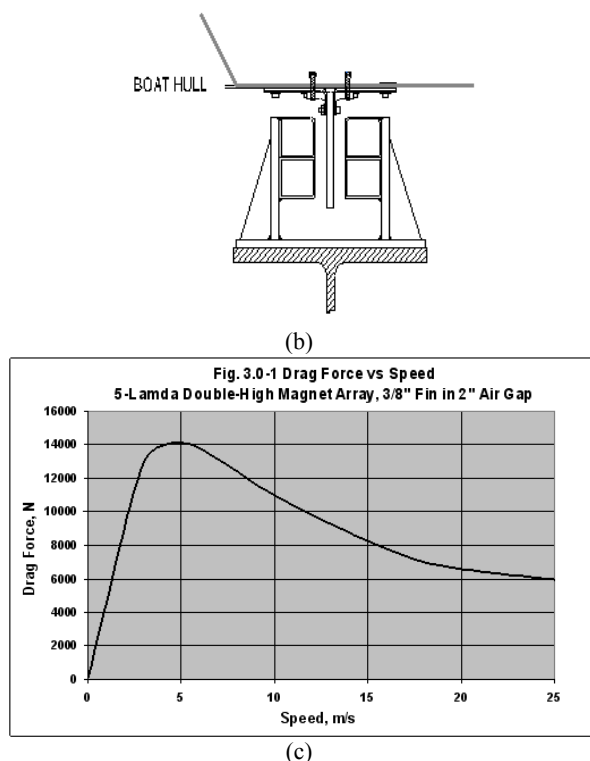

(a)

(b)

(c)
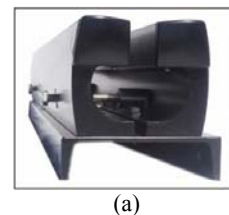
Fig. 13. Eddy current brake (ECB) utilizing NdFeB magnets. (a) Photograph of assembled ECB showing airgap. (b) Use of an ECB in an amusement device. (c) 3D FEA modeling showing braking force vs. speed for an ECB with 3/8" thick copper fin.

V. SUMMARY

This paper provides a framework and design guidelines for the use of NdFeB magnets in large-scale transit, braking and magnetic bearing applications.

ACKNOWLEDGEMENTS

REFERENCES

[1] Z. J. J. Stekly, "Large Scale Applications of Permanent Magnets," *IEEE Transactions on Applied Superconductivity*, vol. 10, no. 1, March 2000, pp. 873-878

[2] J. Evetts, *Concise Encyclopedia of Magnetic and Superconducting Materials,* Pergamon Press, Oxford, 1992

[3] R. J. Parker, *Advances in Permanent Magnetism*, John Wiley, 1990

[4] P. Campbell, *Permanent Magnet Materials and Their Application*, Cambridge University Press, 1994

[5] L. Moskowitz, *Permanent Magnet Design and Application Handbook*, 2nd edition, Krieger Publishing, Malabar FL 1995

[6] S. R. Trout and Y. Zhilichev, "Effective Use of Neodymium Iron Boron Magnets, Case Studies," *Proceedings of the 1999 Electrical Insulation Conference and Electrical Manufacturing and Coil Winding Conference*, Cincinnati, OH, October 26-28, 1999

[7] Y. Kaneko, "Highest Performance of Nd-Fe-B Magnet Over 55 MGOe," *IEEE Transactions on Magnetics*, vol. 36, no. 5, September 2000, pp. 3275-3278

[8] E. P. Furlani, *Permanent Magnet and Electromechanical Devices*, Academic Press, San Diego, 2001

[9] H. C. Roters, *Electromagnetic Devices*, John Wiley, 1941

[10] J.C. Mallinson, "One-Sided Fluxes --- A Magnetic Curiosity?," *IEEE Transactions on Magnetics*, vol. 9, 678-682, 1973 and J.C.Mallinson, H.Shute and D. Wilton, "One-Sided Fluxes in Planar, Cylindrical and Spherical Magnetized Structures" *IEEE Transactions on Magnetics*, vol. 36, no. 2, March 2000, pp. 440-451

[11] K. Halbach, "Design of permanent multipole magnets with oriented rare earth cobalt material," *Nuclear Instruments and Methods*, vol. 169, no. 1, pp. 1-10, 1980

[12] K. Halbach. "Physical and Optical Properties of Rare Earth Cobalt Magnets," *Nuclear Instruments and Methods*, vol. 187. pp. 109-117, 1981

[13] D. L. Trumper, W. Kim and M. E. Williams, "Design and Analysis Framework for Linear Permanent Magnet Machines," *IEEE Transactions on Industry Applications*, vol. 32, no. 2, March/April 1996, pp. 371-379

[14] S. Lang and S. Lee "Design and Analysis of Three Types for Permanent Magnet Linear Synchronous Machine," *IEEE Transactions on Magnetics*, vo1. 38, no. 5, September 2002, pp. 31-33

[15] Z. Q. Zhu and D. Howe, "Halbach Permanent Magnet Machines and Applications: A Review," *IEE Proceedings on Electrical Power Applications*, vol. 148, no. 4, July 2001, pp. 299-308

[16] Q. Han, C. Ham and R. Philips, "Four- and eight-piece Halbach array analysis and geometry optimization for Maglev," *IEE Proceedings on Electrical Power Applications*, vol. 152, no. 3, May 2005, pp. 535-542

[17] R. Kratz and R. Post, "A Null-Current Electro-Dynamic Levitation System," *IEEE Transactions on Applied Superconductivity*, vol. 12, no. 1, March 2002, pp. 930-932

[18] S. Jang, S. Lee and S. Jeong, **"**Characteristic analysis of eddy-current brake system using the linear Halbach array," *IEEE Transactions on Magnetics*, vol. 38, no. 5, September 2002, pp. 2994-2996

[19] M. Kumada et. al., "Development of 4 Tesla Permanent Magnet," *Proceedings of the 2001 Particle Accelerator Conference*, Chicago, 2001

[20] D. Meeker, "Finite Element Method Magnetics (FEMM)," available on web: http://femm.foster-miller.net/wiki/HomePage

[21] J. Ofori-Tenkorang, "A comparative analysis of torque production in Halbach and conventional surface-mounted permanent-magnet synchronous motors," *Proceedings of the IEEE IAS Annual General Meeting*, Orlando, 1995, pp. 657

[22] J. Hoburg, "Modeling Maglev Passenger Compartment Static Magnetic Fields from Linear Halbach Permanent-Magnet Arrays," *IEEE Transactions on Magnetics*, vol. 40, no. 1, Jan. 2004, pp. 59-64

[23] Arnold Magnetic Technologies, information available on web: http://www.grouparnold.com/products/neodymium/pdf/NdFeB.pdf

[24] A. E. Fitzgerald, C. Kingsley, Jr., and S. D. Umans, *Electric Machinery*, 6th edition, McGraw-Hill, 2003

[25] H. F. Mildrum and G. M. Umana, "Elevated Temperature Behavior of Sintered "Nd-Fe-B Type" Magnets," *IEEE Transactions on Magnetics*, vol. 24, no. 2, March 1988, pp. 1623-1625

[26] Arnold Magnetic Technologies, "Temperature Effects on Magnet Output," technical note 0303, June 2003

[27] T. Sebastian, "Temperature Effects on Torque Production and Efficiency of PM Motors using NdFeB Magnets," *IEEE Transactions on Industry Applications*, vol. 31, no. 2, March/April 1995, pp. 353-357

[28] P. Mitchell, "Corrosion Protection of NdFeB Magnets," *IEEE Transactions on Magnetics*, vol. 26, no. 5, September 1990, pp. 1933-1935

[29] Magnet Sales, Inc., information available on web: www.magnetsales.com

[30] V. Zezulka and P. Straka, "Methods of Assembling Large Magnetic Blocks from NdFeB Magnets with a High Value of (BH)max and their Influence on the Magnetic Induction Reached in an Air Gap of a Magnetic Circuit," *IEEE Transactions on Magnetics*, vol. 44, no. 4, April 2008, pp. 485-491

[31] T. Morcos, "The Straight Attraction, Part 2," *Motion Control*, July/August 2000, pp. 24-28

[32] International Commission on Non-Ionizing Radiation Protection, "Guidelines on Limits of Exposure to Static Magnetic Fields," *Health Physics*, vol. 66, no 1, pp 113- 122, 1994

[33] Y. Aoyama, K. Miyata and K. Ohashi, "Simulations and Experiments on Eddy Current in Nd-Fe-B Magnet," *IEEE Transactions on Magnetics*, vol. 41, no. 10, October 2005, pp. 3790-3792

[34] M. Zahn, *Electromagnetic Field Theory: A Problem Solving Approach*, Krieger, 1979

[35] U.S. Department of Transportation (Federal Transit Administration), "The M3 Urban Maglev System," FTA Project Report MA-26-7077, January 8, 2003

[36] R. F. Post, D. D. Ryutov, "The Inductrack: A Simpler Approach to Magnetic Levitation," *IEEE Transactions on Applied Superconductivity*, vol. 10, no. 1, pp. 901-904, March 2000

[37] U.S. Department of Transportation (Federal Transit Administration), "Low Speed Maglev Technology Development Program – Final Report," FTA-CA-26-7025-02.1, March 2002.

[38] S. Gurol and B. Baldi, "Overview of the General Atomics Urban Maglev Technology Development Program," *Proceedings of the 2004 ASMI/IEEE Joint Rail Conference*, April 6-8, 2004, pp. 187-191

[39] T. Clark, A. Kondoleon, M. Thompson and R. Thornton, "Shaftless, Magnetically Levitated Flywheel Energy Storage System," *Aerospace Flywheel Workshop*, Albuquerque NM, October 7-8, 1998

[40] S. Earnshaw, "On the Nature of the Molecular Forces which Regulate the Constitution of the Luminiferous Ether," *Transactions of the Cambridge Philosophical Society.*, vol. 7, pp. 97-112, 1842

[41] E. Pribonic and M. Thompson, "A 21st Century Advancement for Mine Hoisting Systems: Frictionless Non-Powered Emergency Arrestors," *CIM Bulletin*, vol. 101, no. 1107, March/April 2008, pp. 1-8

[42] E. Pribonic and M. Thompson, U.S. Patent 6,523,650, "Permanent magnet eddy brake with flux-steering poles," 2/25/03; U. S. Patent 6,533,083, "Eddy current braking apparatus," 3/18/03 and U. S. Patent 6,918,469, "Curvilinear eddy current braking apparatus," 7/19/05

[43] M. Thompson, "High Temperature Superconducting Magnetic Suspension for Maglev," Ph.D. Thesis. Dept. of Electrical Engineering and Computer Science, Massachusetts Institute of Technology, May 1997

Marc T. Thompson was born on Vinalhaven Island, Maine in 1963. He received the BS, MS, Electrical Engineer's and Ph.D. degrees from the Massachusetts Institute of Technology in 1985, 1992, 1994 and 1997, respectively. Dr. Thompson specializes in custom R/D, analysis, and failure investigations into multi-disciplinary electrical, magnetic, and electronic systems at Thompson Consulting, Inc. (Harvard, MA) and has worked as a consultant at Magnemotion, Magnetar and Magplane, among other companies, following his doctoral work in Maglev at MIT. He has worked as a consultant designing electric motors and generators, and has worked for the USDOT evaluating Maglev and linear motor technologies world-wide. He also is an Adjunct Professor at Worcester Polytechnic Institute (Worcester, MA) where he teaches graduate-level courses in analog, power electronics, magnetic design, electric motors and power distribution. Dr. Thompson is the author of "Intuitive Analog Circuit Design" (Elsevier, 2006) and co-author with Dr. Alexander Kusko of "Power Quality in Electrical Systems," (McGraw-Hill, 2007) and is a contributor of 3 chapters to "Analog Circuits (World-Class Designs), (Elsevier, 2008, edited by Bob Pease) and a contributor of one chapter to Portable Electronics (World Class Designs), (Elsevier, 2009). He has 7 U.S. patents and is a Firefighter with the Harvard, Massachusetts Fire Department.